### Title

Human iPSC-Derived Proinflammatory Macrophages cause Insulin Resistance in an Isogenic White Adipose Tissue Microphysiological System




### Journal

Small, 19(34)

### ISSN

1613-6810



### Authors

Qi, Lin

Matsuo, Koji

Pereira, Ashley

et al.



### Publication Date

2023-08-01

### DOI

10.1002/smll.202203725

Peer reviewed

HHS Public Access

Author manuscript

*Small*. Author manuscript; available in PMC 2024 August 01.

Published in final edited form as:

*Small*. 2023 August ; 19(34): e2203725. doi:10.1002/smll.202203725.

# Human iPSC-derived proinflammatory macrophages cause insulin resistance in an isogenic white adipose tissue microphysiological system

**Lin Qi**,
Department of Nutritional Science and Toxicology, College of Natural Resources, University of California Berkeley, Berkeley, California, 94720, USA

**Koji Matsuo**,
Division of Endocrinology and Metabolism, Institute for Human Genetics, the Eli and Edythe Broad Institute for Regeneration Medicine, and the Program in Craniofacial Biology, Department of Medicine, University of California, San Francisco

**Ashley Pereira**,
Division of Endocrinology and Metabolism, Institute for Human Genetics, the Eli and Edythe Broad Institute for Regeneration Medicine, and the Program in Craniofacial Biology, Department of Medicine, University of California, San Francisco

**Yue Tung Lee**,
Department of Nutritional Science and Toxicology, College of Natural Resources, University of California Berkeley, Berkeley, California, 94720, USA

**Fenmiao Zhong**,
Department of Nutritional Science and Toxicology, College of Natural Resources, University of California Berkeley, Berkeley, California, 94720, USA

**Yuchen He**,
Department of Nutritional Science and Toxicology, College of Natural Resources, University of California Berkeley, Berkeley, California, 94720, USA

**Peter-James H. Zushin**,
Department of Nutritional Science and Toxicology, College of Natural Resources, University of California Berkeley, Berkeley, California, 94720, USA

**Marko Gröger**,
Division of Transplant Surgery, Department of Surgery; Eli and Edythe Broad Center of Regeneration Medicine and Stem Cell Research; Liver Center, University of California, San Francisco

**Aditi Sharma**,

[*]To whom all correspondence should be addressed: astahl@berkeley.edu.

Author contributions

L. Qi designed, performed, and analyzed the main experiments. L. Qi, E.C. Hsiao, H. Willenbring and A. Stahl wrote the manuscript. K. Matsuo, A. Pereira and E. Hsiao focused on iMACs cultivation and analysis. A. Sharma contributed to supplemental data of M2 polarization. M. Gröger assisted iMACs supply. P.J. Zushin synthesized the hydrogel. Y.T. Lee and F. Zhong assisted cell maintenance and imaging analysis. Y.C. He assisted RNAseq data analysis.

Division of Endocrinology and Metabolism, Institute for Human Genetics, the Eli and Edythe Broad Institute for Regeneration Medicine, and the Program in Craniofacial Biology, Department of Medicine, University of California, San Francisco

**Holger Willenbring**,
Division of Transplant Surgery, Department of Surgery; Eli and Edythe Broad Center of Regeneration Medicine and Stem Cell Research; Liver Center, University of California, San Francisco

**Edward C. Hsiao**,
Division of Endocrinology and Metabolism, Institute for Human Genetics, the Eli and Edythe Broad Institute for Regeneration Medicine, and the Program in Craniofacial Biology, Department of Medicine, University of California, San Francisco

**Andreas Stahl***
Department of Nutritional Science and Toxicology, College of Natural Resources, University of California Berkeley, Berkeley, California, 94720, USA

## Abstract

Chronic white adipose tissue (WAT) inflammation has been recognized as a critical early event in the pathogenesis of obesity-related disorders. This process is characterized by the increased residency of proinflammatory M1 macrophages in WAT. However, the lack of an isogenic human macrophage-adipocyte model has limited biological studies and drug discovery efforts, highlighting the need for human stem cell-based approaches. Here, human induced pluripotent stem cell (iPSC) derived macrophages (iMACs) and adipocytes (iADIPOs) are cocultured in a microphysiological system (MPS). iMACs migrate toward and infiltrate into the 3D iADIPOs cluster to form crown-like structures (CLSs)-like morphology around damaged iADIPOs, recreating classic histological features of WAT inflammation seen in obesity. Significantly more CLS-like morphologies formed in aged and palmitic acid-treated iMAC-iADIPO-MPS, showing the ability to mimic inflammatory severity. Importantly, M1 (proinflammatory) but not M2 (tissue repair) iMACs induced insulin resistance and dysregulated lipolysis in iADIPOs. Both RNAseq and cytokines analyses revealed a reciprocal proinflammatory loop in the interactions of M1 iMACs and iADIPOs. Our iMAC-iADIPO-MPS thus successfully recreates pathological conditions of chronically inflamed human WAT, allowing us to study the dynamic inflammatory progression and identify clinically relevant therapies.

### Keywords

organ-on-a-chip; microphysiological system; human induced pluripotent stem cells; white adipose tissue; macrophages; inflammation; insulin sensitivity; iPS cell derived lineages; coculture

## 1. Introduction

Chronic inflammation of white adipose tissue (WAT) is an early event in the pathogenesis of obesity-related disorders causing dysregulated lipolysis and insulin resistance manifesting as decreased uptake of glucose and fatty acid. The resulting elevated serum free fatty acid

levels drive ectopic lipid deposition and organ dysfunction, such as nonalcoholic fatty liver disease (NAFLD) and type-2 diabetes mellitus (T2DM)[1–4]. While WAT normally contains many types of immune cells, macrophages are among the most abundant. In the obese state, WAT signals cause an increase in macrophage mass from ~10% in lean WAT up to 40~50% in obese WAT, with polarization of these macrophages shifting from the M2, mostly associated with tissue repair and anti-inflammatory activities, towards the pro-inflammatory M1 state[5].

Adipocyte-macrophage interactions are complex and not fully understood, involving cytokine signaling, cell-cell contacts, signals from small extracellular vesicles, the exchange of metabolites and even transfer of organelles such as mitochondria[6–9]. Adipose tissue resident macrophages are involved in tissue maintenance and often form crown-like-structures (CLSs) associated with the clearance of damaged adipocytes and lipid droplets but upon activation can also produce high levels of proinflammatory cytokines, such as TNFα and IL6, that ultimately cause insulin resistance in the inflamed WAT[10]. Many current studies investigate macrophage-adipocyte interactions using immortalized cell lines and/or primary cells derived from heterogenic mammalian sources[11–13]. In such systems, xenogeneic or allogeneic immune reactions may interfere with or even mask critical interactions. Few studies have tried to avoid these confounders by relying on autogenic primary cells[14] which are further complicated by the intrinsic fragility and buoyancy of primary adipocytes. These concerns highlight the need for the generation of a robust, isogenic human stem cell-derived adipocyte macrophage system to study critical cell-cell interactions.

Further, many approaches investigating the special interactions between macrophages and adipocytes are static in nature. For example, quantification of CLSs is a classic histological measure to predict metabolic disorder progression but often limited to end-point fixed samples rather than live WAT[15]. As such, the precise temporal sequence of inflammatory cell infiltration into WAT is still unclear[10]. Alternative in vitro approaches are based on plating macrophages directly onto adipocytes in tissue culture plates[16–19]. However, this monolayer model is poorly suited for studying macrophage infiltration and CLSs formation since the structures normally exist in three dimensions. Recent advancements allow coculture of macrophages and adipocytes in 3D self-assembled organoid[14] and hydrogel cultures[14,20]. The 3D environment not only allows macrophages migration and infiltration of adipocyte clusters, but also supports adipogenesis[21], thus emulating the in vivo environment more accurately. However, the approaches used thus far need large amounts of cells and materials. Thus, there is a clear call to create a miniaturized platform that uses stem cell-derived macrophages and adipocytes to reconstruct a 3D WAT.

To address these issues, we modified our previously described iAIDIPO-MPS[22] to create a macrophage (iMAC) plus white adipocyte (iADIPO)-microphysiological system (iMAC-iADIPO-MPS) that supports the 3D coculture of both cell types derived from an isogenic human iPSC line. The iMAC-iADIPO-MPS not only provides a suitable microenvironment supporting iADIPO viability for at least half year, but also allows for real-time observation of iMAC translocation and CLSs formation in 3D, showing its usefulness in predicting metabolic disorder progression.

Using this novel model system, we found that M1, but not M2, macrophages induced insulin resistance and dysregulated lipolysis in iADIPOs. RNAseq and cytokine analyses revealed a reciprocal proinflammatory loop in iMAC-iADIPO interaction. Interestingly, addition of anti-TNFα and anti-IL6 antibodies, or administration of metformin, were able to prevent insulin resistance. Thus, our MPS reconstructs the dynamic inflammatory process in a 3D WAT model using genetically identical macrophages and adipocytes from a single human induced pluripotent stem cell source. Our study provides an isogenic pre-clinical model that may unveil a precise temporal sequence of inflammation in WAT, facilitate drug development, support profound investigation of obesity-related disorders, and advance individualized patient models with the long-term goal of creating “human-on-a-chip” model systems.

## 2. Results

### 2.1 Engineering of iMAC-iADIPO coculture MPS

Based on our previous iADIPO-MPS design, the co-culture MPS was re-engineered to include a straight channel with 300 μm of width for cell loading, which allows for sequential flushing and secondary loading of iMACs (Figure 1a&b). As shown in the schematic, iPSC-MSCs differentiation was induced for 4 days before being loaded into the MPS, then continued for 10 days. During this period, differentiating cells rearranged a biodegradable hyaluronic hydrogel[22] while aggregating in the center of the culture chamber underneath the membrane separating cells from the media channel. This process creates a cell free periphery surrounding the iADIPO cluster. On Day 14, the cell loading channel was flushed with medium to remove excess cells. Then, M1 polarized iMACs were loaded into the MPS under microscopic surveillance to ensure cell delivery into the chamber (Movie S1). The ratio of iMACs:iADIPOs was tuned to 1:5~1:10 based on our preliminary effectiveness tests (Figure S1) and the reported physiological ratios of both cell types in human WAT[5,10]. Immediately after loading, iMACs occupied the space surrounding the iADIPO cluster (Figure 1c). After 12 hours of loading, most of the iMACs migrated toward and into the iADIPO cluster (Figure 1d) resulting in an infiltration of the entire iADIPO cluster (Figure 1e&f). Three days after loading, CLS-like morphology, a histologic hallmark of inflammation and phagocytic removal of dead or dying adipocytes, could be detected (Figure 1g&h, more images in Figure S2). Moreover, spatial interaction between iMACs and iADIPOs can be visualized in 3D by reconstructing confocal scanning images (Movie S2). Together, these results indicate that the iMAC-iADIPO-MPS can recapitulate physiological structures and M1 macrophage-adipocyte interactions.

### 2.2 Diabetic Dysfunction in iMAC-iADIPO-MPS

After 3 days of coculture in the MPS, the metabolic functions of iADIPOs were examined. Coculture of M1 macrophages induced classical markers of insulin resistance in iADIPOs, including failure of insulin to increase uptake of fatty acids or glucose (Figure 2a&b). Further, M1-iADIPOs showed no suppression of lipolysis (Figure 2c), with notable dysregulated basal lipolysis marked by high levels of glycerol release in the absence of β-adrenergic activation (Figure 2c). Conversely, iADIPO-MPS cocultured with M2 macrophages showed insulin sensitive uptake of fatty acid and glucose, as well as normal

lipolysis, similar to iADIPO-MPS cultured without macrophages (Figure 2a–c). Insulin sensitivity was also examined by measuring the phosphorylation of AKT, a central signaling hub downstream of the insulin receptor. As shown in Figure 2d, insulin failed to activate the phosphorylation of AKT at Ser473 in iADIPOs cocultured with M1 macrophages. In contrast, M2 macrophage coculture did not cause significant changes in insulin-activated AKT phosphorylation compared to the group without coculture. As defects in insulin's ability to activate AKT are often linked to the stress- and inflammation-induced c-Jun N-terminal kinases (JNK), we next tested the effects of M1 coculture on JNK activation in iADIPOs. The phosphorylation of JNK at p46 and p46+p54 was significantly increased in iADIPOs after M1 macrophage coculture compared to no coculture condition (Figure 2e). Taken together, these data support the notion that M1 iMAC-iADIPO-MPS display hallmarks of inflamed WAT and accurately reproduced diabetic dysfunction in lipid and glucose metabolism. This provides an isogenic model to study the effects of inflammation in diabetes in a fat-on-a-chip system.

### 2.3 Transcriptional signatures of iMAC-iADIPO interactions

To further study the mechanistic interactions between iMACs and iADIPOs, the two types of cells were cocultured in trans-wells for RNAseq analysis. Since there was little difference in gene clusters between iADIPOs with and without M2 coculture (Figure S3), we focused on a comparison of iADIPOs with M1 versus iADIPOs monoculture. After analysis in DAVID (The Database for Annotation, Visualization, and Integrated Discovery), genes with FDR<0.05 from the cluster with the highest enrichment score (out of 18 clusters) were reviewed. As shown in Figure 3a, iADIPOs cocultured with M1 macrophages significantly upregulated genes associated with immune/inflammatory responses, extracellular space organization, and chemotaxis cytokines. Notably, chemokine-related genes were the most enriched (14~84 fold, Figure 3b). Other enriched categories included the TNF signaling pathway (11 fold) and genes related to extracellular space (3.6 fold). These findings suggest that iADIPOs with M1 coculture were in an inflammatory state, producing chemokines to attract immune cells, regulating angiogenesis[23], and remodeling WAT extracellular matrix. Transcriptional changes by M1 macrophages in response to coculture with or without iADIPOs were less pronounced (Figure 3c&d) showing upregulated cytokine activity (2.53 fold), tumor necrosis factor (8.43/12.6 fold) and its mediated signal pathway (3.26 fold), interferon-gamma production (5.23 fold) and immune responses (2.17 fold). These findings suggest a feed forward loop of proinflammatory cytokine signaling between the M1 macrophages and the iADIPOs which is in line with previous findings of proinflammatory cytokines drives the inflammatory cycle in the WAT.[24] Further, many enriched gene clusters relate to T cells recruitment, indicating the importance of macrophage-adipocyte interaction in shaping the immunological niche in WAT. Genes regulating angiogenesis and extracellular matrix were also upregulated in cocultured M1 macrophages.

Proinflammatory signaling gene expression changes were corroborated by direct measurement of cytokines in the iMACs/iADIPOs coculture media (Figure 3e). In monoculture, M1 macrophages were responsible for producing most of the proinflammatory factors such as TNFα, IL6, IL1β, while iADIPOs produced adipokines and chemokines such as fractalkine and MCP1. Coculture of iMACs and iADIPOs increased production of

multiple cytokines. For instance, INFγ, G-CSF, IL1b, IL1RA, IL10, IL12p40, IL12p70, MIG/CXCL9, and TNFα showed Z-scores of +0.5 ~ +2. Moreover, FGF-2, PDGF-AA, GM-CSF, IL4, IL13, IL22, TNFβ, and VEGF-A in M1-iADIPO coculture, and FGF-2, PDGF-AA, IL8 and IL9 in M2-iADIPO coculture, were dramatically increased with Z-scores greater than +2.

### 2.4 Cytokine driven insulin resistance

To test which of the above identified cytokines can recapitulate the observed insulin resistance, we utilized the iADIPO in a 96-well plate to judge how specific inflammatory cytokines affected metabolic function of the cells. Based on previous publications[25–27] and the high induction of expression, we focused on TNFα, IL6, IL4 and IL1β. After 3 days of treatment with 50 ng/mL TNFα, insulin sensitivity and lipid metabolism of the iADIPOs became similar to that of M1-iADIPO-MPS coculture (Figure 4a–c). IL6 reduced the significant level of insulin responsiveness in both fatty acid and glucose uptake assays, while IL4 and IL1β showed no major impact on insulin sensitivity (Figure 4a&b).

With this focus on TNFα and IL6, we next tested if these two cytokines are required for the M1-induced insulin resistance in iADIPOs by adding neutralizing antibodies against TNFα and IL6 to the M1-iADIPO coculture medium. Intriguingly, 5 ng/mL of a TNFα-specific antibody was efficient to partially prevent M1-induced insulin resistance as measured by insulin stimulated fatty acid uptake (Figure 4d). In contrast, single addition of anti-IL6 failed to significantly rescue insulin resistance. Since TNFα and IL6 act through different signaling mechanisms and IL6 was able to cause insulin resistance (Figure 4a&b), the combination of anti-TNFα and anti-IL6 antibodies (both added at 5 μg/mL) were administrated in the M1-iADIPO-MPS, and robustly restored insulin sensitivity based both on glucose and fatty acid uptake assays. Combination treatment also restored insulin's ability to suppress lipolysis (Figure 4e–g). These results demonstrate that TNFα and IL6 have critical functions in regulating iADIPO insulin sensitivity and show the utility of the M1-iADIPO-MPS platform to interrogate basic biological and clinically relevant functions.

### 2.5 Pharmacological modification of insulin sensitivity in the iMAC-iADIPO-MPS

We used the iMAC-iADIPO-MPS to test the effects of metformin and dexamethasone. Metformin is a widely used insulin sensitizer with not fully understood mode of action that may involve AMPK activation and/or alterations of mitochondrial respiration[28]. Dexamethasone decreases inflammation[29] but also induces insulin resistance in adipocytes[30]. M1-iADIPO-MPS treated with 10 mM metformin showed significantly higher uptake of fatty acids after insulin stimulation compared to basal levels (Figure 5a). Metformin significantly increased insulin stimulated fatty acid uptake in the M1-iADIPO-MPS from 1.08 to 1.62 fold (Figure 5b) but was unable to efficiently restore insulin sensitivity levels observed in the absence of macrophages (2.17 fold). Similarly, metformin treatment increased glucose uptake in the M1-iADIPO-MPS in the presence of insulin (Figure 5c). Interestingly, basal glucose uptake was also enhanced by metformin, as was previously reported in other systems[31], leading to a relatively minor increase in the fold change (Figure 5d). Treatment with 5 μM dexamethasone did not significantly alter insulin

responses in the M1-iADIPO-MPS (Figure 5d) due to either ineffective anti-inflammatory action or/and undesired insulin desensitizing effect.

### 2.6 Modeling pathologies in the iMAC-iADIPO-MPS

To show the ability of our iMAC-iADIPO-MPS to recapitulate known modifiers of adipocyte-macrophage interactions M1 iMACs were cocultured in the iADIPO-MPSs following the creation of two pathological conditions: temporal functional decline, using aged WAT at day 74 (Figure 6b), and obesity-associated cellular hypertrophy of WAT, using adipocytes preincubated with 500 μM of palmitic acid (PA) for 3 days (Figure 6c). For comparison, M1 iMACs were also loaded into standard Day 14 iADIPO-MPS as a control (Figure 6a). Both conditions showed significantly increased lipid droplet numbers and size (Figure 6e). The number of CLS-like morphologies were also significantly increased in “aged” and PA-treated MPS compared to the control (0.28, 0.41 and 0.16 CLS/lipid droplet respectively, Figure 2f). Notably, in the PA-treated condition, many iMACs also contained numerous small lipid droplets resembling the appearance of foam cells, suggesting that the M1 macrophages were actively engulfing released lipids from apoptotic adipocytes (Figure 6d).

## 3. Discussion

Inflammation is a major contributor to adipose tissue dysfunction and metabolic diseases such as obesity, panniculitis, and steatosis. Our understanding of how macrophages and adipocytes interact remains rudimentary because many existing model systems rely on primary cells, often from different donor sources, or are limited due to the large numbers of cells required for the assay. Furthermore, primary adipocytes are difficult to manipulate in the laboratory because of their fragility and buoyancy. An ideal strategy for understanding adipocyte-macrophage interactions would utilize small numbers of highly purified and well characterized cells, in a miniaturized format that would allow for rapid detection and assessment of hormonal and metabolic responses.

Here, we describe the successful application of a unique microphysiologic model system that uses isogenic human iPSC-derived macrophages and adipocytes in conjunction with a dedicated microfluidic platform. We show that the iMAC-iADIPO-MPS recapitulates key features of human WAT/macrophage interactions, including chemokine-driven recruitment of macrophages, formation of CLS-like morphology in 3D, feed-forward pro-inflammatory signaling, and, most importantly, the onset of insulin resistance and dysregulated lipolysis, a combination of features that have not been easily demonstrated using other approaches. Optimized differentiation protocols allowed for the creation of functional iPSC derived macrophages and adipocytes from the same iPSC source, thus alleviating concerns of xeno- and allogeneic immune responses. This represents one of the first 3D cultured human iPSCs-derived macrophage-adipocyte coculture MPS that faithfully recapitulates dynamic inflammation in WAT.

Unlike prior studies that simply attached macrophages to the surface of monolayer adipocytes[17–19] or placed them side-by-side[13,16,32,33], we were excited to find that both M1 and M2 macrophages actively migrated toward and infiltrated into the 3D adipocyte

cluster, assembled as CLS-like morphology, and performed phagocytosis following known physiological patterns. Thanks to the stable stationary microenvironment and the under-the-membrane culture feature[34] in our MPS, the platform ensured adipogenesis[22] and viability of adipocytes for at least half year (Figure S4), showing that long term culture of human adipocytes was feasible and practical. Additionally, due to the use of biodegradable hydrogel matrixes, compact 3D iADIPO clusters were formed in the center of cell chambers providing unoccupied space for macrophage loading. Critically, the system enabled real-time observation of macrophage translocation and CLS formation in three dimensions. The results of CLS quantification also demonstrated the utility of our platform in prediction of metabolic disorder progression. Moreover, the miniaturized system not only saves cells (10~100 fold less) and material compared to conventional 3D culture[22], but also creates a higher cell-to-medium ratio (~$10^{10}$ cells/L) than standard tissue culture (e.g. $10^8$~$10^9$ cells/L), closely matching the human physiology (~$10^{10}$ cells/L[10,35,36]) and avoiding issues with dilutions of secreted cytokines from either cell type. At the same time, we acknowledge limitations of the iMAC-iADIPO-MPS brought about by these low cell numbers and media volumes particularly for subsequent biochemical analysis.

Further, analysis of cytokines in the trans-well cocultures showed that a large number of cytokines were differentially regulated between M1- and M2-iADIPO coculture compared to iADIPO monoculture, indicating a robust interaction between these two cell types. These cytokines can be grouped into three broad categories. First, coculture of M1 and iADIPOs increased proinflammatory factors, such as IL12p40, IL12p70, TNFα and IL1β in the joint medium. Second, cytokine analysis in M1-iADIPO coculture showed the presence of multiple immune cell regulating factors, including INFγ, G-CSF, GM-CSF, MCP-3, and MIG/CXCL9. Similar trends were also observed in M2-iADIPO for increased IL8 and IL9. Finally, both M1- and M2-iADIPO cocultures showed increased production of growth factors, such as FGF-2 and PDGF isoforms and VEGF-A. These findings suggest that iMAC-iADIPO cocultures in our MPS recapitulate aspects of the complex regulatory cytokine network by mutually reinforcing the inflammatory loop, maintaining iMACs polarization and survival, as well as regenerating adipose tissue through adipocyte growth, fibrosis, and angiogenesis[37], which allow us to better dissect the key regulatory pathways of human WAT inflammation.

Interestingly, some samples in M2-iADIPO coculture showed increased IL8 and MIP-1β, suggesting that adipokines from those samples may stimulate M2 cells toward the proinflammatory state. Secondly, we performed additional experiments to address this point by examining the effects of adipocyte conditional media on M2 cytokine secretion. After 2 days culture in such media, the treated macrophages released increased amounts of proinflammatory cytokines, such as IL1beta, IL8, MCP1, and most importantly, the IFNγ, reaching levels comparable to M1 polarized macrophages (Figure S5).

Using our platform, we demonstrated two therapeutic strategies to reduce insulin resistance in glycaemic and lipidemic responses. Although anti-TNFα solely prevented insulin resistance, administration of anti-TNFα and anti-IL6 may be more comprehensive to regain insulin sensitivity in WAT, since the two factors cause insulin resistance through different pathways. IL6 primarily impairs insulin receptor substrate 1 (IRS1) signalling through

STAT3/SOCS3 pathway[45], while TNFα primarily impairs IRS1 through JNK pathway. For the small molecule drugs, metformin is an effective candidate to alleviate insulin resistance, and would be particularly functional in lowering glycaemic level (Figure 5c)[28]. Dexamethasone, however, is ineffective to prevent insulin resistance in either glucose and fatty acid regulation. This may be due to two reasons. First, this drug can directly cause insulin resistance in adipocytes[30], despite its inhibitory effect on inflammation. Second, M1-like macrophages were activated by high doses of LPS and IFNγ which may have rendered them resistant to the anti-inflammatory effects of dexamethasone.

## Conclusion

In summary, we report here the development of a macrophage-adipocyte 3D coculture MPS with cells derived from a single iPSC source and demonstrate its ability to recreate pathological conditions found in chronically inflamed human WAT. The iMAC-iADIPO-MPS provides a unique patient-specific pre-clinical model for studying dynamic inflammatory processes in WAT and provides an attractive method for the interrogation of biological mechanisms and pharmacological interventions of human inflammation and insulin resistance.

## Methods

### MPS fabrication

Fabrication of device followed our previous protocol. Briefly, patterned master templates were fabricated with a thickness of 60 μm by standard photolithography using SU-8 (MicroChem Corp). The cell chambers were circular shape with diameter of 1500 μm due to better adipogenesis support. The microfluidic patterns were replica molded from the master templates to polydimethylsiloxane (PDMS, Sylgard 184, Dow) slabs by soft lithography. The inlet/outlets were holed on the medium channel slab using a 0.75 mm biopsy punch (World Precision Instruments LLC). A polyethylene terephthalate (PET) isoporous membrane (TRAKETCH, SABEU GmbH & Co. KG) was activated by oxygen plasma (Plasma Equipment Technical Services) at 60 W under ~0.6 Torr for 60 s and then chemically decorated in 2% bis(3-(trimethoxysilyl)propyl)anime solution in 97% isopropyl alcohol and 1% Milli-Q water for 30 mins at 80°C. After decoration, the membrane was rinsed in pure isopropyl alcohol and stored in anhydrous ethanol solution until further use. For MPS assembling, the cell chamber and medium channel PDMS slabs were activated by oxygen plasma at 60 W under ~0.6 Torr for 30 s and immediately sandwiched a size-trimmed decorated PET membrane with proper alignment. The device was then baked at 110 °C for 30 mins for ethanol removal, bonding stabilization, and device sterilization.

### Adhesion peptide modified hyaluronic acid synthesis

Modification of hyaluronic acid bases on the previous study of our group[38]. Briefly, hyaluronic acid (65 kDa, Lifecore Biomedical) carrying hydrazide groups was synthesized and then reacted to acryloxysuccinimide to generate acrylate groups. The collagen I short peptide sequence C1[39] (CGGGF(HYP)GER, GenScript), was reacted with the acrylate-HA

at room temperature to form adhesion side chains. After synthesis, the adhesion peptide modified HA precursor was lyophilized until further use.

## Cell culture and differentiation

The human M1 and M2 iMACs were generated using methods detailed in our previous publication[40]. Briefly, iPSCs from the WTC-11 human iPSC line were induced to hematopoietic stem cells using commercial media (STEMdiff™ Hematopoietic Kit, Stemcell Technologies). Floating HSCs were collected and further differentiated toward the human monocyte lineages in RPMI 1640 medium with 10% fetal bovine serum (Avantor Seradigm), 1% penicillin/streptomycin, and 100 ng/mL macrophage-colony stimulating factors (M-CSF). We previously showed that these iMACs were more M2 like, and so these cells were used directly as M2 iMACs. M1 macrophages were obtained by polarizing the M2-like macrophages in culture medium supplemented with 10ng/mL LPS and 20 ng/mL IFNγ for one day prior to use. Differentiation efficiency was approximate 70%. On the day of use, the cells were washed in fresh medium with M-CSF and then magnetically sorted using anti-CD45 coated beads (Miltenyi Biotec) before loading into our coculture system or MPS. Fidelity of iMACs was examined by cytokine profiles. Trace of LPS carryover was also examined by endotoxin assay (E-TOXATE Kit, Sigma Aldrich, Figure S6) to avoid unintended LPS-adipocyte interaction.

Differentiation of iADIPOs were described in our previous study[22]. Briefly, all iPSCs were firstly differentiated into mesenchymal level (iPSC-MSCs) then transfected with exogeneous PPARγ. The iPSC-MSCs were thus chemically inducible for overexpressing PPARγ to enhance adipogenesis. The fidelity and mesenchymal potency of WTC11 iPSC-MSCs was verified previously. For proliferation, iPSC-MSCs were cultivated in a commercial medium (MesenCult-ACF Plus, Stem Cell Technologies) with 30~70% of confluency. For differentiation, cells were grown to confluent with 2 days post-confluent culture. Differentiation was initiated in complete medium (DMEM/F12 containing 1% HEPES, 1% penicillin/streptomycin (all from Gibco) and 10% fetal bovine serum (Equafetal)) with supplements of 0.25 μM dexamethasone, 0.25 mM 3-isobutyl-1-methylxanthine (Sigma-Aldrich), 100 nM rosiglitazone (all from Sigma-Aldrich), 500 nM insulin (Humulin R, Eli Lilly) for 4 days (Day 0 to 3). The rest differentiation was in the complete medium with supplements of insulin and rosiglitazone at the same concentration (Day 4 to the end). Exogeneous PPARγ was expressed by addition of 1 μg/mL doxycycline from Day 0 till the end. A TGF-β pathway inhibitor, SB431542 (abcam), was added into media from Day −2 to Day 14 to prevent chondrogenesis[41]. Final differentiation efficiency is competent to primary adipocytes collected from human biopsy, verified by lipid coverage and gene expression[22].

Coculture of two cells were in iADIPOs medium with supply of 50 ng/mL M-CSF. PA-treated condition was induced by preincubate iADIPO-MPS in 500 μM BSA-complexed palmitic acid (Sigma-Aldrich) for 3 days. For antibodies and drugs testing, anti-TNFα (infliximab, Selleckchem) and anti-IL6 (Sarilumab, Selleckchem), 0.5 μM dexamethasone and 10 mM metformin (Sigma-Aldrich) were added in medium for 2 days of standard tissue culture and 3 days of MPS culture.

### RNAseq sample preparation and data analysis

After coculture of two cells in trans-well settings, macrophages in trans-wells and adipocytes in 24-well culture plates were respectively lysed by TRI Reagent (MilliporeSigma). RNA was purified using the Arcturus PicoPure RNA isolation kit (Applied Biosystems). The RNA yield was examined using the NanoDrop One UV-Vis spectrophotometer (Thermo Scientific). Samples were frozen and shipped in dry-ice to Novogen for RNA-seq analysis. All RNA-seq data were initially analyzed by bioinformatic tools from Novogen to ensure quality control. RNA integrity number (RIN) was reported in Table S1. Genes of interests were then selected based on the relevance to iMAC-iAdipo interaction, and replotted based on data in DAVID analysis (The Database for Annotation, Visualization, and Integrated Discovery). RNAseq analysis was performed by the UCSF Liver Center Bioinformatics core.

### Cytokine analysis

Macrophages and adipocytes were monocultured in 24-well plate or cocultured in trans-well settings with 0.3 mL medium per well for 2 days. Media were all collected and sent to Eve Technologies (Canada) for analysis with Human Cytokine/Chemokines 65-Plex panel (HD65). Cytokines were plotted in heatmap based on fluorescence intensities.

### Immunoblotting

All immunoblotting experiments collected cells from 6-well and 12-well plates. All cocultures were last for 3 days. For phosphorylation of Akt, cells were starved in low glucose DMEM (1g/L glucose, phenol free, Gibco) overnight then stimulated by insulin for 1 hour. After designated treatment, cells were lysed by radioimmunoprecipitation assay (RIPA) buffer with protease and phosphatase and inhibitors (all from ThermoFisher), and centrifuged at 15000 RPM at 4 °C. Protein concentration in cell lysate was quantified by bicinchoninic protein assay (Pierce™, ThermoFisher). Equal amount (20ug) protein was prepared, separated by SDS-PAGE electrophoresis and transferred to polyvinylidene difluoride membrane (all from Bio-Rad). Nonspecific binding was blocked in 5% milk in Tris-buffered saline-tween (TBST) buffer with proper rinse. Specific proteins were stained by monoclonal rabbit 1$^{st}$ antibodies (photspho-Akt Ser 473 #9271, Akt antibody #9272, phospho-SAPK/JNK Thr183/Tyr185 #9251, SAPK/JNK antibody #9252, Cell Signaling Technology) and monoclonal goat 2$^{nd}$ anti-rabbit IgG fluorescent dye with emission wavelength of 800 nm. Reference protein, beta-actin, was labeled at 680 nm. Specific proteins were scanned and quantified under proper settings.

### Culture in MPS

To ensure the adipogenesis of loaded stem cells, the initial stage of differentiation was pre-induced in a tissue culture flask. Differentiating iPSC-MSCs on Day 4, which contain tiny lipid droplets in >80% cells, were dissociated (TrypLE Express, Gibco) and centrifuged as cell pellets. Adhesion peptide modified HA precursor was dissolved in triethanolamine-buffer (TEOA; 0.3 M, pH 8) at a concentration of 3 wt%. Prior to cell loading, 10 wt% MMP cleavable peptides (CQPQGLAKC, GenScript) were dissolved in TEOA and directly added to the cell pellet with dissolved HA precursor under a peptide-to-precursor volume

ratio of 1:10. The hydrogel-cell slurry with density of $8\times10^7$ cells/mL was injected into the cell chamber. To avoid uneven loading density between up- and down-stream cell chambers due to flow resistance, cell slurry was sealed in MPS and equilibrated for 30 mins at room temperature. The MPS was incubated at 37 °C for crosslinking for 30 mins and then connected with catheter couplers (Instech Laboratories) and tubes (Cole-Parmer). Culture medium was infused at a flow rate of 10 μL/hour using a syringe pump (Harvard Apparatus).

After Day 14, the cells in the straight channel and freely floating cells, which were supposed to be poorly differentiated, were flushed out by a continuous medium flow at rate of 30 μL/min. Then iMACs at density of $5\times10^6$ cells/mL were loaded into the cell chamber at flow rate of 5 μL/min. Loaded cell number was estimated based on cell loading density and loading volume. The ratio of iMACs:iADIPOs was controlled at 1:5~1:10 based on our preliminary test (Figure. S1) and physiological ratio in WAT[5,10].

## Hormone-stimulated WAT function assays

Before all assays, adipocytes were subject to serum-free starvation with low glucose DMEM (1g/L glucose, phenol free) overnight. For lipolysis assay, adipocytes were incubated at 37°C in HBSS solution with 0.1% fatty acid free bovine serum albumin (BSA, ThermoFisher) with proper stimulation factors: 1 μM isoproterenol (Sigma-Aldrich), or 1 μM isoproterenol plus 1 μM insulin (Sigma-Aldrich). After 3 hours, the assay solution was collected. The lipolysis progress was determined by measuring glycerol concentration in the collected samples using a commercial reagent (Free Glycerol Reagent, Sigma-Aldrich). For glucose uptake, adipocytes were glucose-free starved using KRPH buffer with 2% BSA prior to test. After 45 mins, adipocytes were incubated in low glucose DMEM without or with 1 μM insulin stimulation at 37°C for 3 hours. The uptake was measured by the clearance of glucose in the medium collected from MPS using Amplex Red kit (ThermoFisher Scientific) following manufacture's instruction. Briefly, medium in each chip was collected and diluted to 50 μL then incubate with 50 μL of Amplex Red reagent containing glucose oxidase and horseradish peroxidase. Glucose thus enzymatically generates hydrogel peroxide that react with the reagent resulting in red-fluorescent product resorufin. After 30 min at room temperature, resorufin was measured in absorbance at 560 nm. For the fatty acid assay in the device, HBSS solution with 0.1% BSA, additional 3.5 g/mL glucose, and 1 μM Bodipy 3823 were infused into the medium channel at a flow rate of 20 μL/min, a much higher rate to ensure mixing and delivery efficiency. The entire system was placed in an incubation tank (Zeiss) with 5% $CO_2$ supply and 37°C heating. The uptake was monitored using a fluorescence microscope in resolution of 2048 pixels × 2048 pixels at designated time points up to 30 mins. Focal length was tuned to ~10 μm to reduce fluorescence out of adipocyte cluster. Fatty acid uptake was calculated based on the increase of fluorescent intensity of entire adipocyte cluster after a certain period, in unit of relative fluorescence unit per time, and pairwisely normalized to the basal uptake of each sample for comparison purpose. For the fatty acid uptake in culture plate, 3mM Trypan Blue was added to quench extracellular Bodipy. Each well of 96-well plate were screened by 20 flashes yielding averaged fluorescent intensity. Insulin stimulated and basal uptake groups were respectively from eight wells

### Fluorescence staining

Cell viability was justified by staining live cells with 2 μM calcein AM and dead cells with 4 μM ethidium homodimer-1 (Invitrogen) in HBSS for 15 mins. All images were captured within 1 hour in the microscope-associated incubation tank. Live iMACs were traced by pre-staining their cytoplasm in serum-free culture medium with 10 μM blue CMAC dye (CellTracker™, C2110, ThermoFisher) before dissociating and loading. Lipid droplets of live iADIPOs were labeled in DM2 with 1 μM fluorescent fatty acid (Bodipy D3823) for 2 days. For the purpose of morphology investigation, adipocytes were firstly fixed by 4% paraformaldehyde for 2 hours in the MPS. Nuclei, lipid droplets, and F-actin, were respectively stained by 300 nM DAPI (ThermoFisher), 1 μM Bodipy D3922 (ThermoFisher), and 1 phalloidim-iFluor 647 (abcam) in PBS with 1% BSA overnight. Samples were mounted (Diamond Antifade, Invitrogen) after staining and rinsing. Pre-coculture cell membrane staining of live adipocytes were also separately tested (CellMask Deep Red, Invitrogen). After macrophage coculture, as shown in Figure S5, cell membrane seems similar to Figure 1. Considering that the pre-coculture staining of adipocytes may induce extra cell damage or stress to fragile adipocytes that may interfere the interaction between macrophages and adipocytes, we only pre-stained macrophages with CMAC dye, which has been widely used in immune cells[42–44].

### Characterizations

Bright-field and fluorescent images were captured by a wide-field fluorescence microscope (AxioObserver Z1, Zeiss) and confocal fluorescence microscopes (LSM710, LSM880, Zeiss). Captured images were save in .czi files to access original parameters and then processed in either Zen-black (2.3 SP1 FP3 64bit) on microscope-associated computer or Zen-blue (3.4 version, used as downloaded) on other Windows computers. Processing bases on image histogram to eliminate background/autofluorescence from image and adapt the brightest bar less than 1~3% of the entire image. Within defined histogram range, images were preferably tuned to be brighter for better visional effect. Due to lack of Zen-software support on MacOS, ImageJ (1.53a, used as downloaded, no plug-ins or macros add-on) was only to analyze Tiff images exported from Zen-software (e.g. counting cells, circle cell contour, both did manually and automatically to ensure accuracy). To measure time-lapsed fluorescence change, the look-up-table and other imaging settings were kept consistent. CLS-like morphologies were quantified by measuring the number of unilocular lipids with more than 80% perimeter surrounded by iMACs (Figure S7). Absorbance and fluorescence of assay solutions were read by a microplate reader (SpectraMax i3x, Molecular Devices). Western blotting images were obtained by Odyssey Infrared Imager and analyzed with Image Studio Lite (LI-COR Biosciences).

### Statistics

All experiments have been reproduced for at least 3 times, with biological replicates derived from independent samples (n). Only those samples showing hugely varied values (i.e. a few outliers, detecting by quantile method) were performed again and we only showed new result without technical replicates. In our graph, dots represent the values of each biological replicate and mean values were calculated from independent samples. All results from the

TC condition were obtained from at least 3 biological replicates, i.e. different samples from the same batch of experiment. Lipid size analysis based on images of at least 10 cell chambers from 3 chips in each group. Lipid size in the largest bin of size distribution histogram was sorted and analyzed. There are 2~6 lipids counted in the largest bin. Number of bins (K) was determined based on Sturge's rule: K=1+3.322log(n), where n is number of observed lipids per analysis (typically 100~300 lipid per group). Noting that lipid size was also measured using other calibers (Figure S8), while they were not representative enough for lipid size in mature adipocytes due to interference of tiny lipids from multilocular or apoptotic adipocytes. All western blotting analyses bases on 3 biological replicates. For the in-MPS glucose and lipolysis assays, the results were obtained from at least 3 independent groups, where each group combines the assay solution collected from 2 chips, and each chip contained 8 cell chambers. For the in-MPS fatty acid uptake assay, the images of each condition were taken from 8 cell chambers at the same time. In experiments that need to quantify stimulation-induced indexes, basal and stimulated conditions were sequentially assayed and sampled from the same chip to reduce variance. The cell number in MPS is estimated based on cell density in every loading then multiply loading volume. All results were statistically analyzed by JMP 11 (SAS Institute) or Prism (GraphPad). Two-tailed student t-test with assumption of equal variance was used to compare the difference between two groups. P-value <0.05 was evaluated as significant (*), <0.005 as highly significant (**). Results were presented in average values. Error bars represent standard derivation in each group. All experiments were independently reproduced for at least 3 times.

## Supplementary Material

Refer to Web version on PubMed Central for supplementary material.

## Acknowledgements

This study was supported by NIH grant 1UG3DK120004. E.C. Hsiao also received support from the Robert L. Kroc Chair in Rheumatic and Connective Tissue Diseases III and NIH R01066735. LQ was supported by a postdoctoral fellowship from the Siebel Stem Cell Institute. K. Matsuo was supported by Mochida Memorial Foundation for Medical and Pharmaceutical Research and the Uehara Memorial Foundation. Confocal imagines were captured at the CRL Molecular Imaging Center, RRID:SCR_017852, supported by Gordon and Betty Moore Foundation. Bioinformatic analysis was performed by the Liver Gene Analysis Core of the UCSF Liver Center (P30 DK26743).

### Competing interests

E.C. Hsiao receives funding from Ipsen Pharmaceuticals for clinical trials that are not related to this study. ECH serves in a volunteer capacity on the International Clinical Council on FOP, the Medical Advisory board of the FD/MAS Foundation, and the IFOPA Medical Registry advisory board. E.C. Hsiao is also on the editorial board of the Journal of Bone and Mineral Research. There is no competing interest to declare.

## References

1. Haffner SM Pre-diabetes, insulin resistance, inflammation and CVD risk. Diabetes research and clinical practice 61 Suppl 1, S9–S18, doi:10.1016/s0168-8227(03)00122-0 (2003). [PubMed: 12880690]
2. Santoro A, McGraw TE & Kahn BB Insulin action in adipocytes, adipose remodeling, and systemic effects. Cell metabolism 33, 748–757 (2021). [PubMed: 33826917]
3. Birkenfeld AL & Shulman GI Nonalcoholic fatty liver disease, hepatic insulin resistance, and type 2 diabetes. Hepatology 59, 713–723, doi:10.1002/hep.26672 (2014). [PubMed: 23929732]

4. Cusi K The role of adipose tissue and lipotoxicity in the pathogenesis of type 2 diabetes. Current diabetes reports 10, 306–315, doi:10.1007/s11892-010-0122-6 (2010). [PubMed: 20556549]
5. Weisberg SP et al. Obesity is associated with macrophage accumulation in adipose tissue. The Journal of clinical investigation 112, 1796–1808 (2003). [PubMed: 14679176]
6. Nitta CF & Orlando RA Crosstalk between immune cells and adipocytes requires both paracrine factors and cell contact to modify cytokine secretion. PloS one 8, e77306 (2013). [PubMed: 24204798]
7. Keuper M On the role of macrophages in the control of adipocyte energy metabolism. Endocrine Connections 8, R105–R121 (2019). [PubMed: 31085768]
8. Zhou Z, Tao Y, Zhao H & Wang Q Adipose extracellular vesicles: Messengers from and to macrophages in regulating immunometabolic homeostasis or disorders. Frontiers in Immunology 12 (2021).
9. Brestoff JR et al. Intercellular mitochondria transfer to macrophages regulates white adipose tissue homeostasis and is impaired in obesity. Cell metabolism 33, 270–282. e278 (2021). [PubMed: 33278339]
10. Rosen ED & Spiegelman BM What we talk about when we talk about fat. Cell 156, 20–44 (2014). [PubMed: 24439368]
11. Eguchi A et al. Microparticles release by adipocytes act as “find-me” signals to promote macrophage migration. PloS one 10, e0123110 (2015). [PubMed: 25849214]
12. Kongsuphol P et al. In vitro micro-physiological model of the inflamed human adipose tissue for immune-metabolic analysis in type II diabetes. Scientific reports 9, 1–14 (2019). [PubMed: 30626917]
13. Liu Y et al. Adipose-on-a-chip: a dynamic microphysiological in vitro model of the human adipose for immune-metabolic analysis in type II diabetes. Lab Chip 19, 241–253 (2019). [PubMed: 30566152]
14. Taylor J et al. Generation of immune cell containing adipose organoids for in vitro analysis of immune metabolism. Scientific reports 10, 1–14 (2020). [PubMed: 31913322]
15. Geng J et al. 3D microscopy and deep learning reveal the heterogeneity of crown-like structure microenvironments in intact adipose tissue. Science Advances 7, eabe2480 (2021). [PubMed: 33597245]
16. Suganami T, Nishida J & Ogawa Y A paracrine loop between adipocytes and macrophages aggravates inflammatory changes: role of free fatty acids and tumor necrosis factor α. Arteriosclerosis, thrombosis, and vascular biology 25, 2062–2068 (2005). [PubMed: 16123319]
17. Lee Y-H, Kim S-N, Kwon H-J, Maddipati KR & Granneman JG Adipogenic role of alternatively activated macrophages in β-adrenergic remodeling of white adipose tissue. American Journal of Physiology-Regulatory, Integrative and Comparative Physiology (2016).
18. Furuhashi M et al. Adipocyte/macrophage fatty acid–binding proteins contribute to metabolic deterioration through actions in both macrophages and adipocytes in mice. The Journal of clinical investigation 118, 2640–2650 (2008). [PubMed: 18551191]
19. Chen X et al. Necroptosis in macrophage foam cells promotes fat graft fibrosis in mice. Frontiers in cell and developmental biology 9 (2021).
20. Park SB et al. Development of in vitro three-dimensional co-culture system for metabolic syndrome therapeutic agents. Diabetes, Obesity and Metabolism 21, 1146–1157 (2019).
21. Hsiao AY, Okitsu T, Teramae H & Takeuchi S 3D tissue formation of unilocular adipocytes in hydrogel microfibers. Advanced healthcare materials 5, 548–556 (2016). [PubMed: 26680212]
22. Qi L et al. Probing Insulin Sensitivity with Metabolically Competent Human Stem Cell-Derived White Adipose Tissue Microphysiological Systems. Small, 2103157 (2021).
23. Zhu Q, Han X, Peng J, Qin H & Wang Y The role of CXC chemokines and their receptors in the progression and treatment of tumors. Journal of molecular histology 43, 699–713 (2012). [PubMed: 22752457]
24. Liu R & Nikolajczyk BS Tissue immune cells fuel obesity-associated inflammation in adipose tissue and beyond. Frontiers in immunology 10, 1587 (2019). [PubMed: 31379820]

25. Sárvári A et al. Interaction of differentiated human adipocytes with macrophages leads to trogocytosis and selective IL-6 secretion. Cell death & disease 6, e1613–e1613 (2015). [PubMed: 25611388]
26. Lacasa D, Taleb S, Keophiphath M, Miranville A & Clement K Macrophage-secreted factors impair human adipogenesis: involvement of proinflammatory state in preadipocytes. Endocrinology 148, 868–877 (2007). [PubMed: 17082259]
27. Juge-Aubry CE et al. Regulatory effects of interleukin (IL)-1, interferon-β, and IL-4 on the production of IL-1 receptor antagonist by human adipose tissue. The Journal of Clinical Endocrinology & Metabolism 89, 2652–2658 (2004). [PubMed: 15181037]
28. Barbe P, Millet L, Galitzky J, Lafontan M & Berlan M In situ assessment of the role of the β1, β2- and β3-adrenoceptors in the control of lipolysis and nutritive blood flow in human subcutaneous adipose tissue. British journal of pharmacology 117, 907–913 (1996). [PubMed: 8851509]
29. Tsurufuji S, Sugio K & Takemasa F The role of glucocorticoid receptor and gene expression in the anti-inflammatory action of dexamethasone. Nature 280, 408–410 (1979). [PubMed: 460415]
30. Sakoda H et al. Dexamethasone-induced insulin resistance in 3T3-L1 adipocytes is due to inhibition of glucose transport rather than insulin signal transduction. Diabetes 49, 1700–1708 (2000). [PubMed: 11016454]
31. Fischer M et al. Metformin induces glucose uptake in human preadipocyte-derived adipocytes from various fat depots. Diabetes, Obesity and Metabolism 12, 356–359 (2010).
32. Spencer M et al. Adipose tissue macrophages in insulin-resistant subjects are associated with collagen VI and fibrosis and demonstrate alternative activation. American Journal of Physiology-Endocrinology and Metabolism (2010).
33. Herroon MK, Diedrich JD & Podgorski I New 3D-culture approaches to study interactions of bone marrow adipocytes with metastatic prostate cancer cells. Frontiers in endocrinology 7, 84 (2016). [PubMed: 27458427]
34. Harms MJ et al. Mature human white adipocytes cultured under membranes maintain identity, function, and can transdifferentiate into brown-like adipocytes. Cell reports 27, 213–225. e215 (2019). [PubMed: 30943403]
35. Tomlinson DJ, Erskine RM, Morse CI & Onambélé GL Body fat percentage, body mass index, fat mass index and the ageing bone: their singular and combined roles linked to physical activity and diet. Nutrients 11, 195 (2019). [PubMed: 30669348]
36. Sharma R & Sharma S Physiology, Blood Volume. (StatPearls Publishing, Treasure Island (FL), 2021).
37. Crewe C, An YA & Scherer PE The ominous triad of adipose tissue dysfunction: inflammation, fibrosis, and impaired angiogenesis. The Journal of clinical investigation 127, 74–82 (2017). [PubMed: 28045400]
38. Jha AK et al. Matrix metalloproteinase-13 mediated degradation of hyaluronic acid-based matrices orchestrates stem cell engraftment through vascular integration. Biomaterials 89, 136–147 (2016). [PubMed: 26967648]
39. Knight CG et al. The Collagen-binding A-domains of Integrins α1β1 and α2β1recognize the same specific amino acid sequence, GFOGER, in native (Triple-helical) collagens. J Biol Chem 275, 35–40 (2000). [PubMed: 10617582]
40. Matsuo K et al. ACVR1R206H extends inflammatory responses in human induced pluripotent stem cell-derived macrophages. Bone 153, 116129 (2021). [PubMed: 34311122]
41. Pfeifer CG et al. TGF-β Signalling is Suppressed under Pro-Hypertrophic Conditions in MSC Chondrogenesis Due to TGF-β Receptor Downregulation. International journal of stem cells 12, 139 (2019). [PubMed: 30836731]
42. Catron DM, Pape KA, Fife BT, Van Rooijen N & Jenkins MK A protease-dependent mechanism for initiating T-dependent B cell responses to large particulate antigens. The Journal of Immunology 184, 3609–3617 (2010). [PubMed: 20208013]
43. Gupta S et al. T cell receptor engagement leads to the recruitment of IBP, a novel guanine nucleotide exchange factor, to the immunological synapse. J Biol Chem 278, 43541–43549 (2003). [PubMed: 12923183]

44. Montoya MC et al. Role of ICAM-3 in the initial interaction of T lymphocytes and APCs. Nature immunology 3, 159–168 (2002). [PubMed: 11812993]

45. Rehman Kanwal, et al. Role of interleukin-6 in development of insulin resistance and type 2 diabetes mellitus. Critical Reviews™ in Eukaryotic Gene Expression 27.3 (2017).

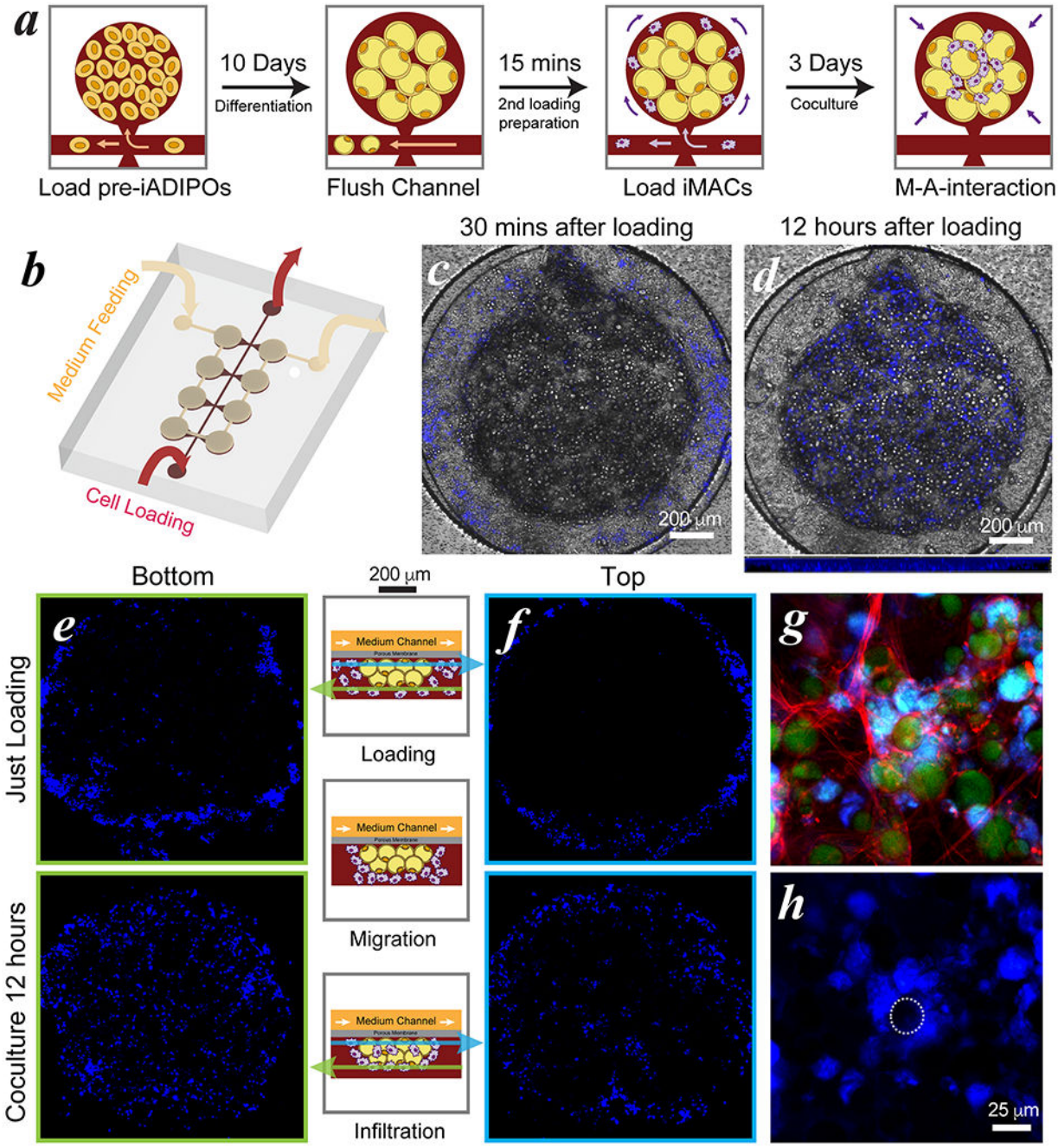


**Figure 1. Engineering of iMAC-iADIPO coculture MPS.**

(a) coculture procedure. (b) Schematic of chip design. (c)&(d) iMACs distribution after 30 min and 12 hours of loading. Confocal images captured from the focal planes at (e) bottom & (f) top of iADIPO clusters immediately after loading and after 12 hours coculture. (g)&(h) A typical crown-like structure formed after coculture in MPS. iMACs were labeled in blue; lipids of iADIPOs were labeled in green, F-actin of both cells was labeled in red. Circle in (h) indicate one of the CLS-like morphology.

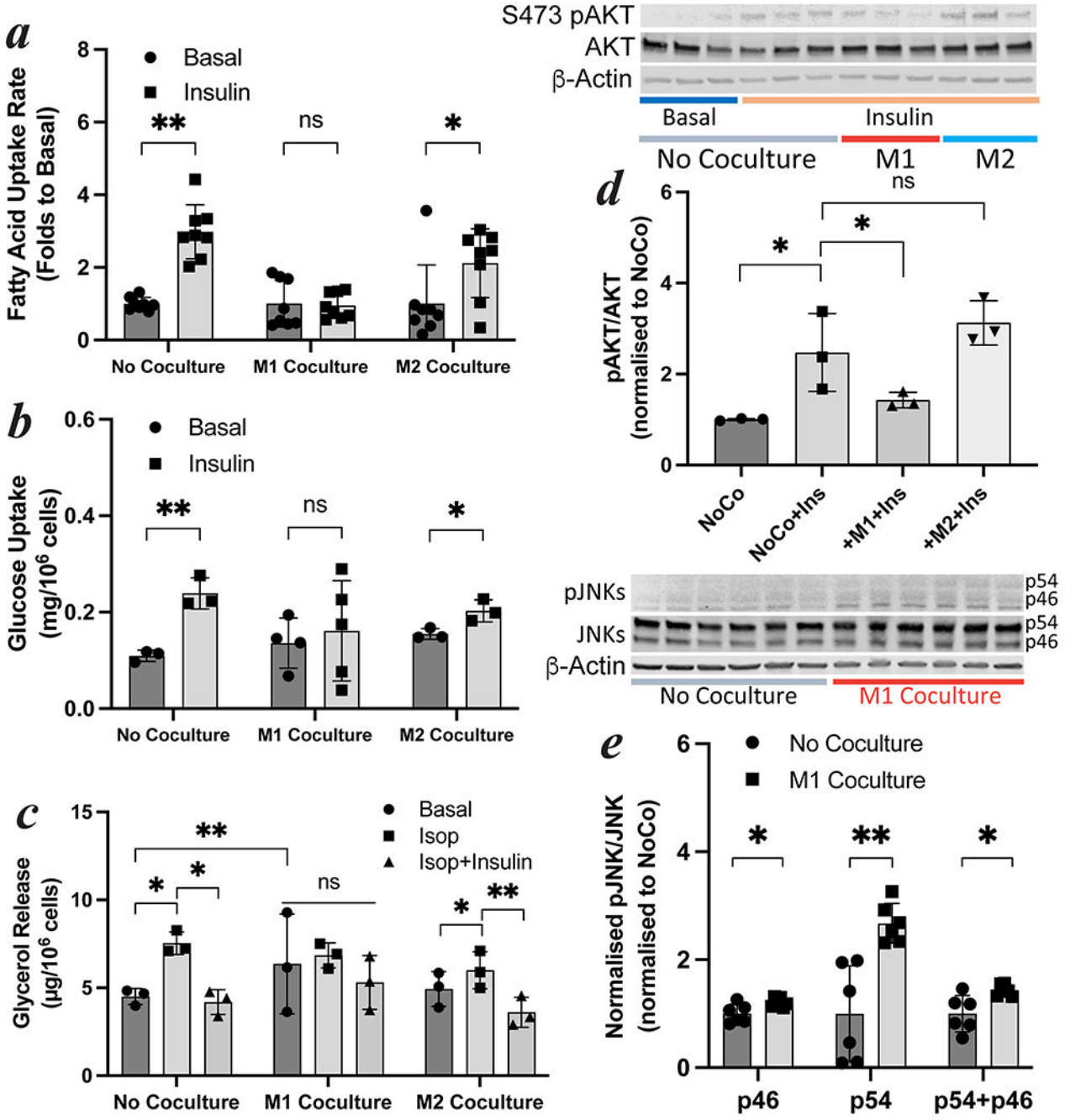


**Figure 2. Dysregulated metabolic functions in iMAC-iADIPO-MPS.**

M1 but not M2 caused insulin resistance in uptakes of (a) fatty acid and (b) glucose, and also caused (c) dysregulated lipolysis process. (d) Phosphorylation of Akt (PKB) in response to insulin after M1 and M2 coculture. (e) Phosphorylation of JNK after M1 coculture. All cocultures were last for 3 days. N=8 in (a) and N>3 in (b)&(c). *: $p<0.05$, **:$p<0.005$, ns: $p>0.05$. P-values were determined by two-tails t-test with assumption of equal variance. (a)-(c) were performed in MPS and (d)-(e) in plate culture. Glucose uptake based on

the clearance of glucose in the media. Dots represent the measured values of biological replicates.

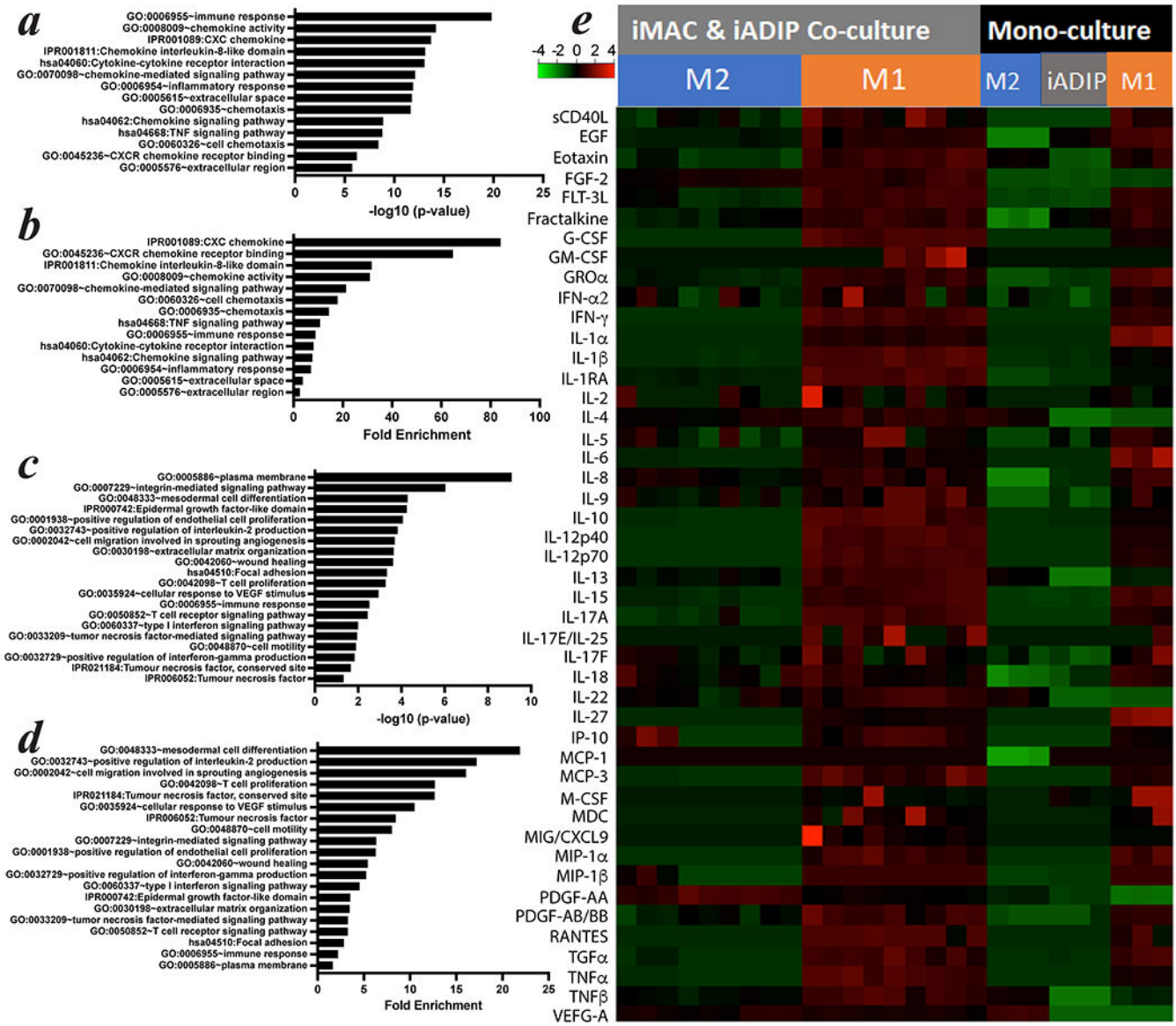


**Figure 3. Transcriptional signatures in coculture of iMACs and iADIPOs.**

RNA-seq analysis of iADIPOs after M1 vs. M2 coculture shown in (a) −log10 of p-value and (b) upregulated folds. All selected genes were from the group with highest enrichment score in clustering analysis (out of 18). RNA-seq analysis of M1 iMACs after iADIPO coculture vs. monoculture shown in (c) −log10 of p-value and (d) upregulated fold. (e) Cytokine profiles of M1 and M2 coculture with iADIPOs and their respective monocultures. All cocultures were performed in trans-well culture plate settings and last for 2 days. N=3 in each group.

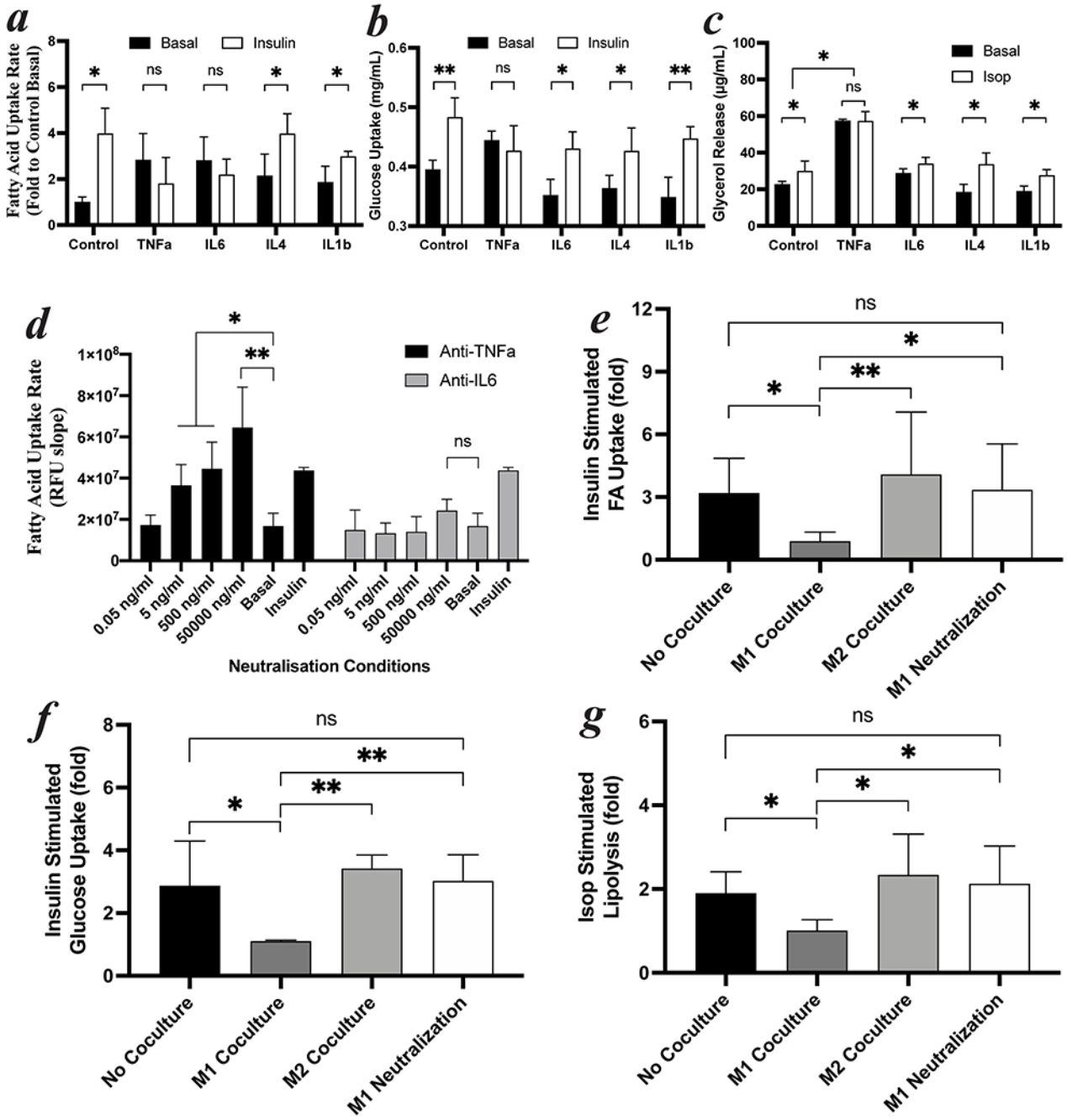


**Figure 4. Cytokine caused insulin resistance.**

(a) Fatty acid uptake, (b) glucose uptake and (c) lipolysis of iADIPOs after 3 days treatment of selected cytokines at 50 ng/mL. (d) Effectiveness of antibodies specific to TNFα and IL6 on insulin sensitivity of iADIPOs after M1 coculture. (e)-(g) Cocktail of anti-TNFα and anti-IL6 cocktail maintained hormonal responsiveness of iADIPOs in measure of insulin stimulated (e) fatty acid uptake, (f) glucose uptake and (g) isoproterenol stimulated lipolysis. (a)-(d) were performed in 96-well culture plate for identifying key cytokines and establishing conditions, N=4. (e)-(g) were performed in coculture MPS. N=8 in (e). N>3 in

(f)&(g). *: $p<0.05$, **: $p<0.005$, ns: $p>0.05$. P-values were determined by two-tails t-test with assumption of equal variance.

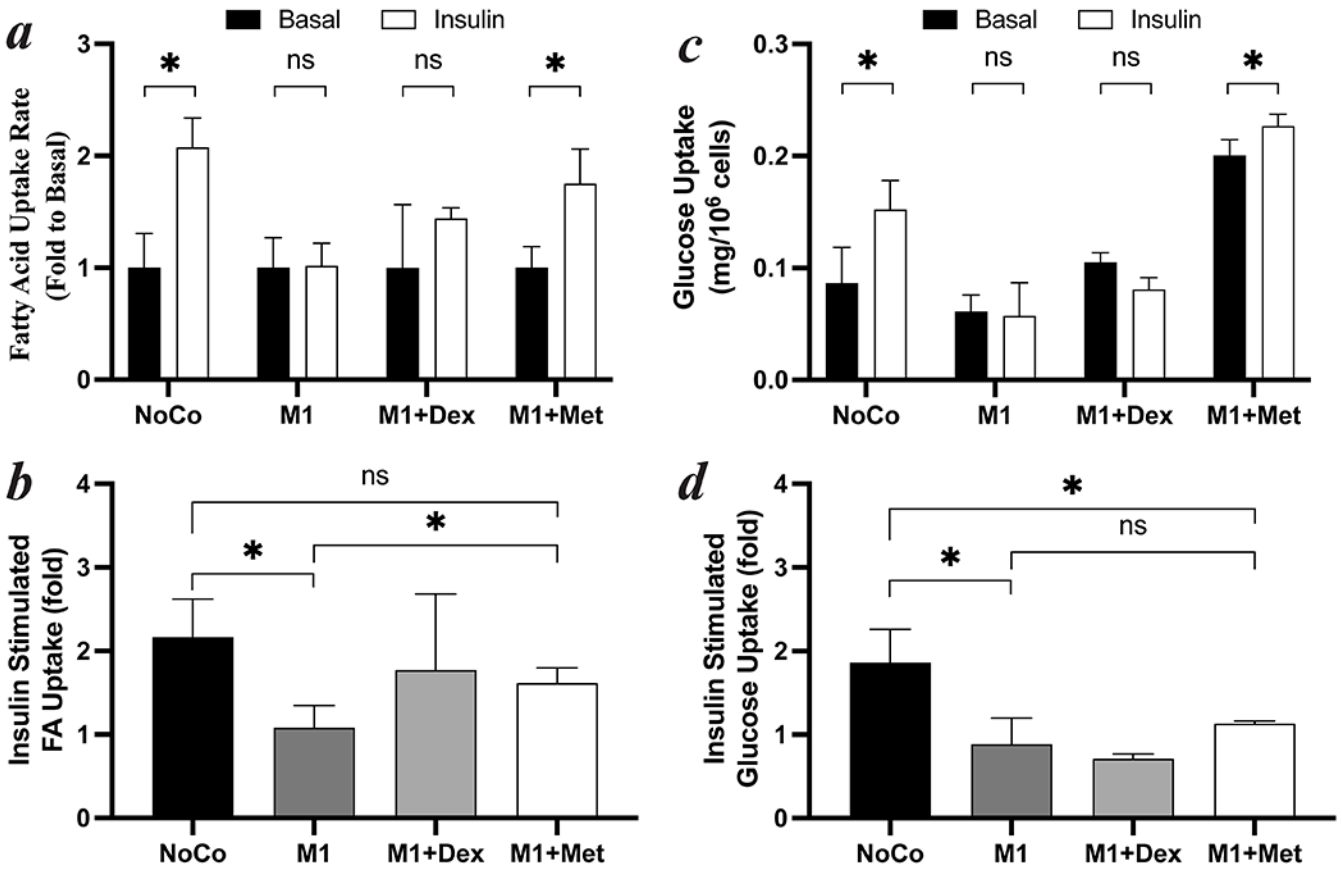


**Figure 5. Pharmacological modification of insulin sensitivity in M1-iADIPO-MPS.**

(a) Fatty acid uptake and (b) index. (c) Glucose uptake and (d) index. Dexamethasone and metformin were administrated immediately after M1 iMACs loading. N=3 for all. *: $p<0.05$, **: $p<0.005$, ns: $p>0.05$. P-values were determined by two-tails t-test with assumption of equal variance. All were performed in MPS.

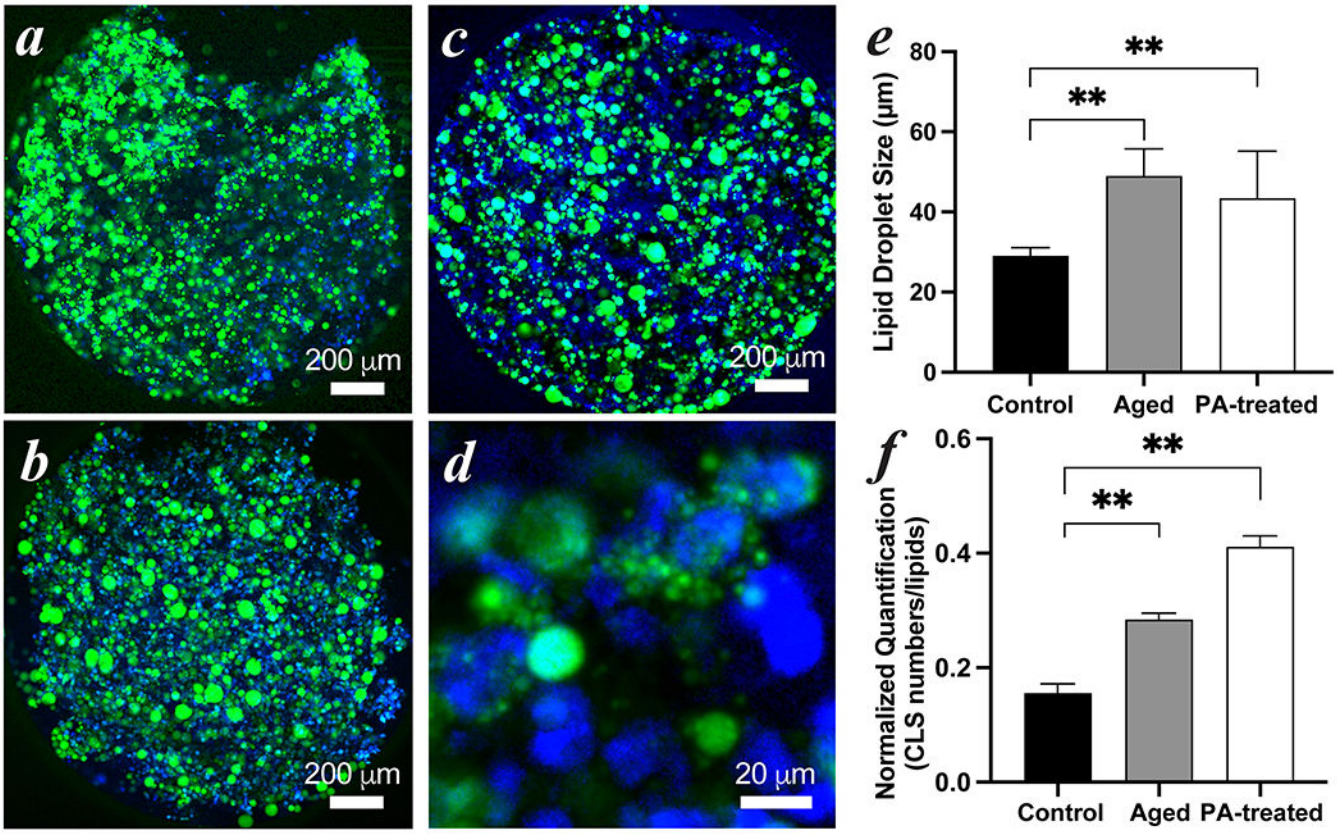


**Figure 6. Simulated inflammation in iMAC-iADIPO-MPS.**

(a) standard (Day 14), (b) aged (Day 74) and (c) PA-treated (Day14 after 3 days of 0.5 mM palmitic acid treatment) conditions. (d) shows a typical zoomed-in view in PA-treated condition. (e) lipid size and (f) CLS-like morphology quantification of three conditions. iMACs were labeled in blue. Lipids of iADIPOs were labeled in green. CLS-like morphology was quantified based on criterion that >80% of an iADIPO was surrounded or covered by iMACs. N=10 (thus 60 data points) per group in (e) and N>3 in (f). *: $p<0.05$, **: $p<0.005$, ns: $p>0.05$. P-values were determined by two-tails t-test with assumption of equal variance. All were performed in MPS.